

## Status of ISMRAN experiment

---

**Pawan Kumar Netrakanti,<sup>a,\*</sup> K. Kumar,<sup>a,b</sup> S. P. Behera,<sup>a</sup> R. Sehgal,<sup>a</sup> D. K. Mishra,<sup>a,b</sup>  
V. Jha<sup>a,b</sup> and L. M. Pant<sup>c,b</sup>**

<sup>a</sup>*Nuclear Physics Division, Bhabha Atomic Research Centre, Mumbai, INDIA*

<sup>b</sup>*Homi Bhabha National Institute, Anushakti Nagar, Mumbai, INDIA*

<sup>c</sup>*Technical Physics Division, Bhabha Atomic Research Centre, Mumbai, INDIA*

E-mail: [pawankn@barc.gov.in](mailto:pawankn@barc.gov.in)

Indian Scintillator Matrix for Reactor Anti-Neutrino (ISMRAN) experiment is the first indigenous effort in the country to measure the reactor based antineutrinos at very close distances (~13 m) from the reactor core. The experiment is setup in DHRUVA research reactor and has been in the data taking mode since January 2022. The main goal of ISMRAN is to understand the Reactor Anti-neutrino Anomaly from a reactor core, which utilizes natural uranium as fuel. All previous measurements are performed using highly enriched  $^{235}\text{U}$  fuel and observed a deficit of 4-6% in the antineutrino yield when compared with theory predictions. In this proceedings, we present first results from the complete ISMRAN setup at DHRUVA reactor hall. We will summarize the foreground activities that were carried out for the understanding of the ISMRAN detector response. A new generation of experiments for future, involving the measurement of reactor antineutrinos using coherent elastic scattering will also be discussed.

*16th International Conference on Heavy Quarks and Leptons (HQL2023)  
28 November-2 December 2023  
TIFR, Mumbai, Maharashtra, India*

---

\*Speaker

## 1. Introduction

The measurement and study of reactor antineutrinos ( $\bar{\nu}_e$ ) have addressed very important aspects of neutrino physics in terms of their detection, oscillation parameters, and fuel compositions. Experimental collaborations such as Daya Bay [1], RENO [2], and Double Chooz [3] have achieved detailed and precise measurements of  $\bar{\nu}_e$  energy spectrum and mixing angle  $\theta_{13}$ . However, comparisons between theoretical models and experimental results observe a  $\sim 6\%$  deficit in global reactor  $\bar{\nu}_e$  flux, known as "reactor antineutrino anomaly" (RAA) [4]. This deficit can be attributed to either an improper treatment of  $\bar{\nu}_e$  flux from the reactor [5] or the oscillation of three flavor oscillating neutrinos to sterile neutrinos. Initial estimates of the reactor  $\bar{\nu}_e$  rates by Huber [6] and Mueller [7] model calculations suggested a deficit of  $\sim 6\%$ , when compared with experimentally measured data. With recent improvements in the reactor flux calculations, the deficit has now been reduced to 2-3% [5]. When studied the shape of the reactor  $\bar{\nu}_e$  spectra as a function of energy, there is an excess of yield observed in the 5-7 MeV region when compared with theoretical models. The HKSS model gives a partial explanation of the 5 MeV bump by taking into account forbidden  $\beta$  decays [8]. However, many ongoing efforts for the search of eV-scale sterile neutrinos at very short baseline experiments ( $\sim 10\text{cm}$ ) have reported significant exclusions in the parameter space of mixing angle ( $\sin^2(2\theta_{14})$ ) and mass difference ( $\Delta m_{41}^2$ ) between the sterile and active neutrinos. These experiments are also sensitive to monitor the reactor power in a non-intrusive way and estimate the fuel composition as a function of burn up [9, 10].

To understand and address some of the above mentioned aspects, an array of plastic scintillator bars (PSBs) known as Indian Scintillator Matrix for Reactor Anti-Neutrinos (ISMRAN), has been installed and commissioned at the Dhruva research reactor facility, comprising of natural uranium as fuel, at  $\sim 13\text{ m}$  from the reactor core at Bhabha Atomic Research Centre (BARC). The reactor  $\bar{\nu}_e$ 's will be measured by using the inverse beta decay (IBD) process and the measured spectra may be used for the search of sterile neutrino with a mass on the order of  $\sim 1\text{ eV}/c^2$  [11]. At the same time, the monitoring of the reactor thermal power and fuel evolution [12, 13] can be demonstrated using the measured  $\bar{\nu}_e$  yields as a function of time.

In this proceedings, we present the recent progress and status of ISMRAN experiment at Dhruva reactor hall. Initial measurements were carried out at a distance of  $\sim 13\text{ m}$  and were encountered by huge background from the nearing neutron guide tube. The experiment is successfully relocated, at a distance of  $\sim 18\text{ m}$ , to the newer site inside the reactor hall, where the relative background is almost 7 times less than the previous site. With the measurements from the new site, a very preliminary  $\bar{\nu}_e$  spectra has been presented. Also, improvements in the detection efficiency of  $\bar{\nu}_e$  is demonstrated using a machine learning technique to discriminate fast neutron background from the measured prompt energy spectra.

## 2. ISMRAN experiment

Dhruva is a research reactor with thermal power capacity of  $100\text{ MW}_{\text{th}}$ , which is utilized for the basic science research using thermal neutrons. Apart from basic science, the production of radioisotopes for medical applications is also key feature of the reactor. A very short baseline experiment, ISMRAN is setup in Dhruva research reactor at Bhabha Atomic Research Centre,

Mumbai. The experiment is currently placed at the distance of  $\sim 18$  m from the reactor core. A schematic diagram of the experiment is shown in Fig. 1. An array of 90 PSBs is surmounted on a movable base structure. The PSBs are shielded from the external  $\gamma$ -rays and neutrons using 10 cm of lead and 10 cm boronated polyethylene sheets, respectively. The outermost layer consists of muon veto detector covering from all sides to reject the cosmic muons and to tag muons induced backgrounds. In the current setup at Dhruva reactor hall, the muon veto system is not installed and the rejection of cosmic muon background is done using the signal deposition in the PSBs only. Each PSB has a dimension of  $10\text{ cm} \times 10\text{ cm} \times 100\text{ cm}$ , wrapped with Gadolinium Oxide ( $\text{Gd}_2\text{O}_3$ ) coated on aluminized mylar foils. The areal density of the  $\text{Gd}_2\text{O}_3$  on these foils is  $4.8\text{ mg/cm}^2$ . The signal from the PSBs is read out using 3" photomultiplier tubes (PMT) coupled directly to the bars. The active detector component approximately weighs 1 ton. The anode signals are read and fed directly to the digitizer's for further signal processing. The ISMRAN experiment uses 12 CAEN V1730 digitizers for the signal processing. Each digitizer consist of 16 channels, with 4 FPGA's that can process the baseline subtraction, constant fraction discrimination, threshold selection, event triggering, and timestamping of the recorded events. A 14-bit flash ADC is used for the integral charge measurement for the energy reconstruction in bars.

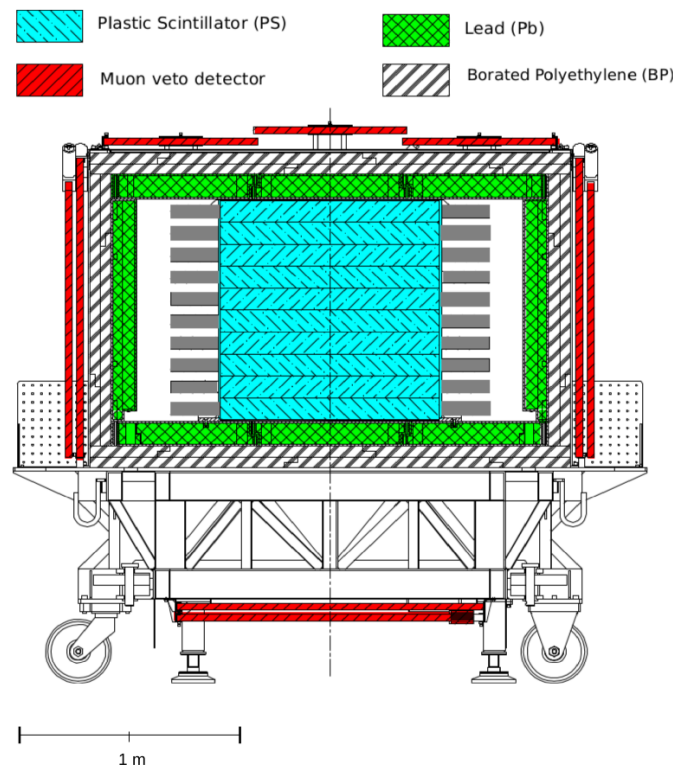
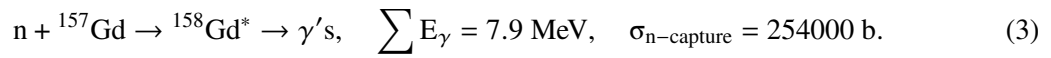


**Figure 1:** Schematic diagram of the full scale ISMRAN detector setup consisting of 90 PSBs. The detector array is surmounted on a movable base structure and is shielded by 10 cm of lead and 10 cm of boronated polyethylene sheets all around.

The detection of  $\bar{\nu}_e$  events in ISMRAN PSB is done using IBD process.



In this process the  $\bar{\nu}_e$  interacts with the protons in the hydrogen atom of the plastic scintillator material and produces a positron and a neutron as shown in Eq. 1. To balance the reaction kinematics, the positron carries most of the  $\bar{\nu}_e$ 's energy and hence acts as a proxy signature for the energy measurements. The drawback of detecting  $\bar{\nu}_e$  via IBD is the threshold energy of 1.8 MeV, which restricts the detection of reactor  $\bar{\nu}_e$ 's below this threshold. The positron being a charged particle losses its energy instantly in the PSBs and annihilates with the surrounding electron to produce a pair of  $\gamma$ -rays with energy equals to 0.511 MeV each. The combination of positron energy loss and annihilation  $\gamma$ -rays forms the prompt signal. On the other hand, the neutron shares very small energy (few KeV's) and thermalizes in the plastic scintillator medium. Eventually it gets captured either on Gd or H. The capture cross-section for Gd is very high and from the simulation the neutron is estimated to be captured  $\sim 75\%$  of the times in the ISMRAN like geometry. The neutron capture on Gd and de-excitation of Gd nucleus results in emission of cascade of  $\gamma$ -rays, with a total energy equivalent to  $\sim 8$  MeV. The neutron capture on two different isotopes of Gd which have highest capture cross-section are shown in Eqs. 2 and 3.



While the neutron capture on H results in emission of monoenergetic  $\gamma$ -ray of 2.2 MeV. The neutron capture signal represents the delayed signal. The characteristic time difference between the prompt and delayed signals in ISMRAN geometry is estimated to be  $\sim 68 \mu\text{s}$  from Geant4 simulation. Figure 2 shows the schematic representation of a typical IBD event in ISMRAN experiment.

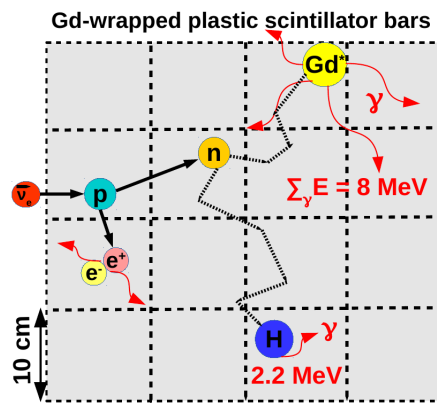


**Figure 2:** Representation of a typical IBD event inside ISMRAN detector. Also shown are the positron prompt event and neutron captured delayed event.

### 3. ISMRAN detector response

To understand the response of PSBs, a detailed characterization of each bar is done in non-reactor environment for the estimation of charge deposition, timing measurements, and position parameterization. The energy response of PSBs are studied using  $\gamma$ -rays from radioactive sources and cosmic muons, as shown in Fig. 3 (a), (b), and (c) panels. The results are compared with simulations using Geant4 where the detector geometry, physics processes for different interactions and implementation of digitization of the energy deposition in each bar is performed to get a reasonable agreement with the measured data [14]. The uniformity of the response among all the

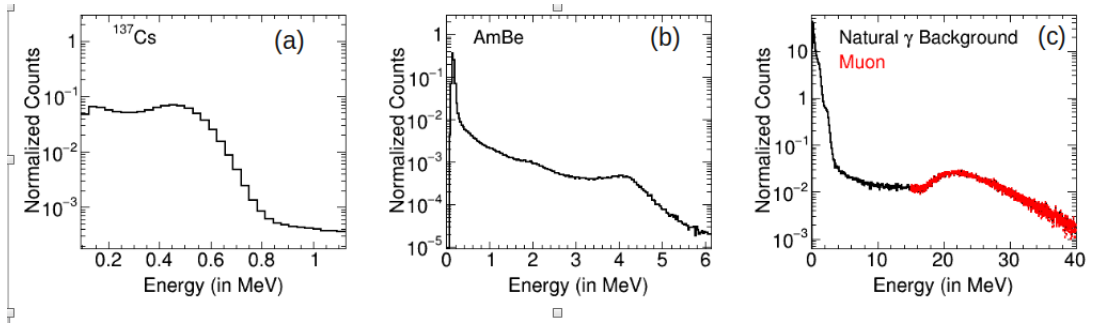


**Figure 3:** Energy response of PSB for (a)  $\gamma$ -ray, (b) AmBe neutron source, and (c) cosmic muons.

PSBs is estimated to be within  $\sim 2\%$ . Figure 4 (a) and (b) show the energy resolution and energy scale measured in one PSB for different  $\gamma$ -ray radioactive sources. The energy resolution is fitted to an empirical function which takes into account the noise, stochastic and statistical fluctuation of photoelectron collection. The typical energy resolution obtained for PSB varies as  $14\%/\sqrt{E}$ . The energy scale improves with increasing energy. To understand the event reconstruction, we use the

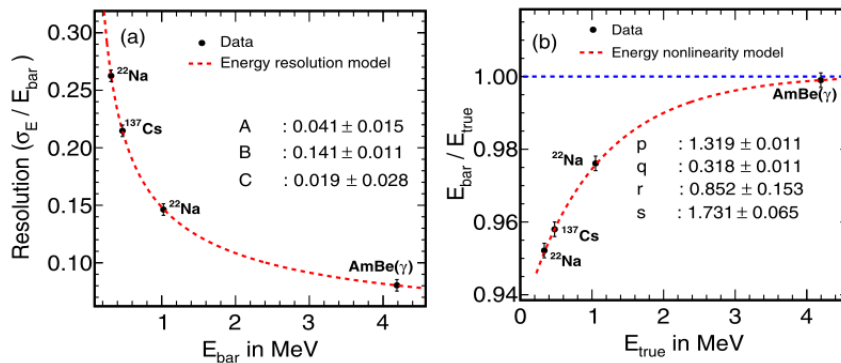


**Figure 4:** Energy resolution and scale of PSB using  $\gamma$ -ray sources as a function of incident  $\gamma$ -energies.

neutron capture event on Gd foils. The implementation of cascade  $\gamma$ -ray distribution in Geant4 is not well modelled. An external package DICEBOX is used to model the cascade  $\gamma$ -rays [15]. Figure 5 (a), (b), and (c) show the individual  $\gamma$ -ray energy response from the cascade emission, energy sum of  $\gamma$ -rays from one cascade, and the number of bars hits in one cascade event from

the Am-Be source. The results from data are compared with Geant4 simulations and both agree reasonably well.

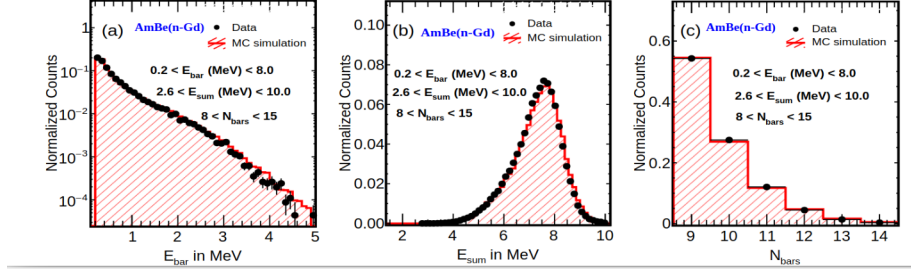


**Figure 5:** Comparison of data and MC simulation results for (a) individual  $\gamma$ -ray energies, (b) sum energy of the cascade  $\gamma$ -rays, and (c) number of PSBs hit in one event from n-Gd capture cascade event.

#### 4. Background for ISMRAN experiment

Due to an above ground experiment, ISMRAN faces harsh backgrounds from cosmic muons, neutrons,  $\gamma$ -ray and fast neutron background from the reactor. The cosmic muon background is handled by vetoing the events which occur within  $250 \mu\text{s}$  of the passage of muons. The natural and reactor  $\gamma$ -ray background is discriminated by taking timing distribution selection on the prompt and delayed event. One of the irreducible backgrounds is from the fast-neutrons which mimic the IBD event signature. The fast neutron undergoes proton recoil in PSB, which mimics the prompt signal and the same neutron then thermalizes and gets captured in Gd foils giving a delayed signal. The characteristic time of IBD and fast neutron event are very similar and hard to discriminate. We

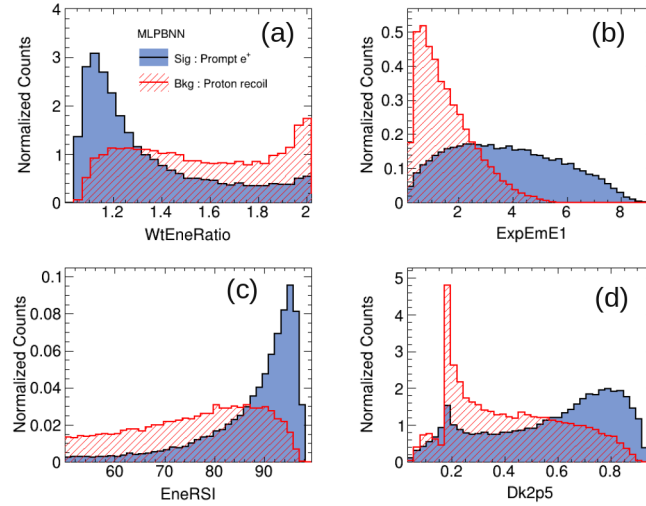


**Figure 6:** Variables constructed from the sum energy, number of bars hit, and energy profile ( $E_{\text{max}}$  and  $E_1$ ) on event by event basis for IBD signal and fast neutron background events.

exploit the segmented geometry of ISMRAN detector to discriminate the fast neutron background

from IBD events using a machine learning approach. We use different variables, as shown in Fig. 6 (a)-(d), which are constructed from the sum energy, number of bars hit and energy deposition profile ( $E_{\max}$  and  $E_1$ ) on event by event basis. The prompt signal from IBD and fast neutron exhibit characteristic differences in energy deposition profile [16]. These variables are selected from a variety of other variables and gives the best discriminatory powers. For machine learning, we use the likelihood estimator and a multi-layer perceptron using Bayesian neural network (MLPBNN) algorithm for the discrimination of signal and background events. Figure 7 shows the ROC curve for fast neutron background rejection fraction as a function of positron detection efficiency. A modest efficiency of 48% can be achieved with a fast neutron background rejection of over 93%.

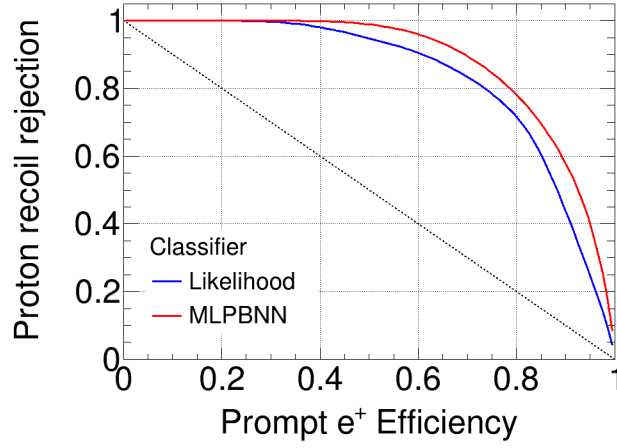


**Figure 7:** ROC curve for likelihood estimator and MLPBNN algorithm for proton recoil event rejection as a function of positron efficiency.

## 5. $\bar{\nu}_e$ candidate events

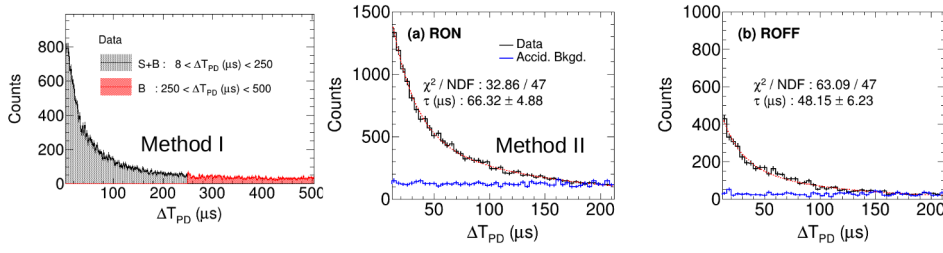


**Figure 8:** Timing difference  $\Delta T_{PD}$  between prompt and delayed events. Also shown are the signal (black) and accidental background (red) regions along with purely reconstructed accidental background (blue) for reactor ON and OFF conditions.

After incorporating the background rejection criteria for cosmic muons, fast neutrons, and  $\gamma$ -rays, the prompt and delayed candidate events are filtered according to the sum energy and number

of bars hit. A fiducial volume is defined where there is no hit in the outermost layer of ISMRAN PSB. The timing difference ( $\Delta T_{PD}$ ) distribution between prompt and delayed events are shown in Fig 8. Signal with background (S+B) events are considered in the range of  $8 < \Delta T_{PD} (\mu s) < 250$  and accidental background (B) events from  $250 < \Delta T_{PD} (\mu s) < 500$  range. Figure 8 (a) and (b) show the  $\Delta T_{PD}$  for prompt and delayed event pairs for reactor ON and OFF data, respectively. The data are fitted with exponential with a constant background function. For reactor ON data, the characteristic time ( $\tau$ )  $66.32 \pm 4.88 \mu s$  that is close to neutron capture time obtained from simulations. For OFF condition, the  $\tau$  obtained from fit is  $48.16 \pm 6.23 \mu s$ , which may be due to correlated backgrounds that are present in the reactor hall. Also shown are the accidental event contribution, which are constructed by shifting the prompt event timestamp by 2 ms and prompt-delayed pairs are constructed with these shifted events. These are termed as mixed events and are only used for the determination of accidental background. The advantage of using such a technique is to overcome the statistical fluctuations in the B region to overcome background subtraction biases. The constant nature of the distribution in both RON and ROFF indicates the randomness of the events generated from the purely accidental background within the selected time window for the prompt and delayed event reconstruction. To obtain  $\bar{\nu}_e$  events, we use two methods of background

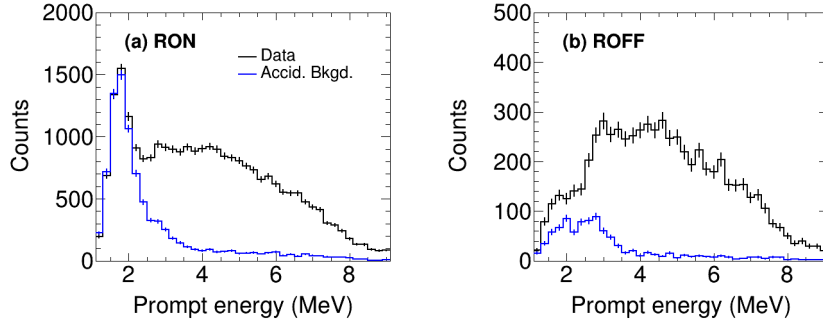


**Figure 9:** Sum energy projection of prompt events in (a) RON and (b) ROFF condition. Also shown are the prompt sum energy for accidental events (blue) histograms.

subtraction. These methods are described in Eqs. 4 and 5,

$$N_{\bar{\nu}_e}^I = [ ( N_{RON}^R(S+B) - N_{RON}^R(B) ) - K ( N_{ROFF}^R(S+B) - N_{ROFF}^R(B) ) ], \quad (4)$$

$$N_{\bar{\nu}_e}^{II} = [ ( N_{RON}^R(S+B) - N_{RON}^M(S+B) ) - K ( N_{ROFF}^R(S+B) - N_{ROFF}^M(S+B) ) ], \quad (5)$$

where  $N_{\bar{\nu}_e}^I$  and  $N_{\bar{\nu}_e}^{II}$  are the number of  $\bar{\nu}_e$  events obtained from method I and method II.  $N_{RON}^R(S+B)$  and  $N_{ROFF}^R(S+B)$  are the number of events in the S+B region for real event pairs in RON and ROFF condition, respectively. Similarly,  $N_{RON}^R(B)$  and  $N_{ROFF}^R(B)$  are the number of events in B region for real event pairs in RON and ROFF condition. In method II, instead of using background from real event pairs in the B region, we select the events from the mixed events in the S+B region. The K in both equations denote the normalization factor for number of RON days to that of number of ROFF days. We have compared the distribution of background events in B region from real event pairs with those which are obtained from mixed event technique in the S+B region. Within available statistics they are comparable.

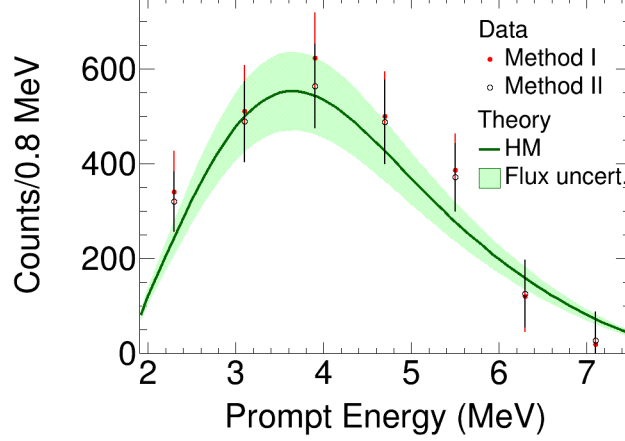


**Figure 10:** Very preliminary prompt energy spectra from RON data compared with the expectations from HM calculations.

## 6. Results and discussion

Figure 9 (a) and (b) show the sum energy projection for prompt events in the  $\Delta T_{PD}$  window for (S+B) and (B) regions for RON and ROFF conditions, respectively. Also shown, in blue histograms, are the sum energy distributions from the mixed events for the accidental background. The relative background's are subtracted according to Eqs. 4 and 5 to obtain the background subtracted prompt energy distributions. Figure 10 shows the background subtracted prompt energy distribution of data analyzed for 41 RON days. The results obtained from both method I and II are in reasonable agreement within the available statistics. Also shown is the prediction obtained from the HM model and the uncertainty in the  $\bar{\nu}_e$  flux, as shown in green band, in assigned. The reported results are for the nominal reactor power at  $77 \text{ MW}_{th}$  at a distance of 18m from the reactor core. The integrated  $\bar{\nu}_e$  yield obtained from method I and II are  $2499 \pm 224$  (stat) and  $2382 \pm 203$  (stat) and are slightly lower from the expectation from the HM model of  $2639 \pm 52$  (stat). With ISMRAN in continuous data taking mode, we expect to increase the current statistics and improve our results in terms of  $\bar{\nu}_e$  spectra in next six months.

## 7. Summary and outlook

We report the first reactor antineutrino measurements, in the country, from ISMRAN experiment obtained from DHRUVA reactor. The ISMRAN detector was successfully tested and installed in the reactor hall and has been taking physics data since August 2023. The characterization of the detectors is performed in a non-reactor environment and the setup has been benchmarked with radioactive source, neutron source, and cosmic muons. A thorough background estimation and rejection are implemented in the experimental data for the removal of fast neutron,  $\gamma$ -ray, and muon related backgrounds. A very preliminary result for the rate of reactor antineutrinos is obtained with two subtraction methods and are in reasonable agreement with each other, further ensuring the

robustness of the analysis techniques. We are working on the improvement of our results in terms of statistical uncertainties by taking data for longer duration and would be able to measure antineutrino spectra more precisely. A detailed estimation of systematic uncertainties from various sources are in progress and will be reported soon. For the future, new generation experiments are been planned to be setup in Apsara-U research reactor. The detector setup would utilize the inorganic crystals in cryogenic temperatures to measure the coherent neutrino nucleus elastic scattering. The experimental site has been finalized and procurement is in full swing for the detector element and simulations for shielding for future experiments.

## 8. acknowledgement

We thank the Reactor Operations Division, Research Reactor Safety Division, and Center for Design and Manufacturing from BARC who have helped us in setting up ISMRAN experiment.

## References

- [1] F. P. An et al. (Daya Bay Collaboration), *Phys. Rev. Lett.* 108 (2012) 171803.
- [2] J. K. Ahn et al. (RENO Collaboration), *Phys. Rev. Lett.* 108 (2012) 191802.
- [3] Y. Abe et al. (Double Chooz Collaboration). *Phys. Rev. Lett.* 108 (2012) 131801.
- [4] G. Mention et al. *Phys. Rev. D* 83 (2011) 073006.
- [5] C. Giunti, Y. F. Li, C. A. Ternes and Z. Xin, *Phys. Lett. B* 829 (2022) 137054.
- [6] P. Huber, *Phys. Rev. C* 84 (2011) 024617.
- [7] Th. A. Mueller et al., *Phys. Rev. C* 83 (2011) 054615.
- [8] L. Hayen, J. Konstensalo, N. Severijns, and J. Suhonen *Phys. Rev. C* 100 (2019) 054323.
- [9] N. S. Bowden et al., *Nucl. Instr. Meth. in Phys. Res., Sect. A* 572 (2007) 985.
- [10] G. Boireau et al., (Nucifer Collaboration). *Phys. Rev. D* 93 (2016) 112006.
- [11] S. P. Behera, D. K. Mishra, and L. M. Pant, *Phys. Rev. D* 102 (2020) 013002.
- [12] Technical Meeting on Nuclear Data for Anti-neutrino Spectra and Their Applications, 23-26 April 2019, IAEA Headquarters, Vienna, Austria.
- [13] S. Oguri et al., (PANDA Collaboration), *Nucl. Instr. Meth. in Phys. Res., Sect. A* 757 (2014) 33-39.
- [14] R. Dey, P. K. Netrakanti, et. al. (ISMRAN Collaboration) *Nucl. Instr. Meth. in Phys. Res., Sect. A* 1042 (2022) 167415.
- [15] F. Becvar, *Nucl. Instr. Meth. in Phys. Res., Sect. A*, 417 (1998) 434.
- [16] D. Mulmule, P. K. Netrakanti, L. M. Pant, and B. K. Nayak. *JINST*, 15 (2020) P04021.